Supporting Information

In Situ Constructed $Ni_3S_2/CoMo_2S_4$ Heterointerface on Nickel Foam for Efficient Bifunctional Water Splitting

Baoling Zou[a], Fozia Sultana[a], Qiurong Wang[a], Renkun Li[a], Ting Xiao[a], Xiaojing Liu[a], Tongtong Li[b,*], Renhong Li[a,*]

[a] State Key Laboratory of Bio-based Fiber Materials, Zhejiang Sci-Tech University, Hangzhou, 310018, China

[b] Department of Materials Science & Engineering, Zhejiang Sci-Tech University, Hangzhou, 310018, China

[*]Corresponding author.

E-mail addresses: lirenhong@zstu.edu.cn (R. Li), yitaji@zstu.edu.cn (T. Li)

Characterization

The crystal structures were analyzed by X-ray diffraction (XRD, Shimadzu XRD-6100) using Cu Kα radiation ($\lambda = 1.5418$ Å) over a 2θ range of 5–90°. The morphology was examined using field-emission scanning electron microscopy (FE-SEM, ZEISS Ultra Plus). Detailed microstructural information was obtained using transmission electron microscopy (TEM) and high-resolution TEM (HRTEM, JEOL EM002B). Elemental distribution was analyzed by energy-dispersive X-ray spectroscopy (EDS) attached to the TEM. Surface chemical states and elemental composition were characterized by X-ray photoelectron spectroscopy (XPS, JEOL JPS-9010MC). All binding energies were calibrated with respect to the C 1s peak at 284.8 eV. The bulk elemental composition was quantified by inductively coupled plasma optical emission spectrometry (ICP-OES, Agilent) to determine the metal stoichiometry.

Electrochemical measurements

All electrochemical measurements performed on a CHI660E electrochemical workstation (Shanghai Chenhua) using a standard three-electrode configuration. The as-prepared catalyst grown in situ on nickel foam (NF) served directly as the working electrode, with an average mass loading of ~3.0 mg. A Hg/HgO electrode and a carbon rod were used as the reference and counter electrodes, respectively.

All measurements were conducted in 1.0 M KOH electrolyte at room temperature. Prior to testing, the electrolyte was purged with N_2 for 30 min to remove dissolved gases. Continuous stirring was applied during measurements to facilitate bubble release and prevent blockage of active sites. The OER and HER activities were evaluated by linear sweep voltammetry (LSV) at a scan rate of 5 mV s^{-1}. All polarization curves were corrected with 90% iR compensation. Tafel slopes were derived from the Tafel equation:

$$\eta = a + b * \log j \quad (1)$$

where η is the overpotential, j is the current density, and b represents the Tafel slope.

Electrochemical impedance spectroscopy (EIS) was conducted in the frequency range of 0.01–10^5 Hz with an amplitude of 5 mV. The electrochemical double-layer capacitance (C_{dl}) was determined from cyclic voltammetry (CV) curves recorded in the non-faradaic region (1.0–1.1 V vs. RHE) at scan rates of 20, 40, 60, 80, and 100 mV s^{-1}. The electrochemically active surface area (ECSA) was estimated according to:

$$ECSA = C_{dl}/C_s \quad (2)$$

where C_s represents the specific capacitance.

For stability evaluation, chronopotentiometry was performed in 1.0 M KOH at current densities of 50 mA cm^{-2} for OER and 10 mA cm^{-2} for HER. Additionally, 2000 cyclic voltammetry (CV) cycles were conducted at 100 mV s^{-1}, followed by LSV measurements to assess activity retention. Prior to formal testing, the electrodes were activated by 20 CV cycles at 20 mV s^{-1}.

All potentials were converted to the reversible hydrogen electrode (RHE) using:

$$E_{RHE} = E_{Hg/HgO} + 0.059 \times pH + 0.098 \quad (3)$$

The overpotential (η) for OER was calculated as:

$$\eta = E_{RHE} - 1.23 \quad (4)$$

The mass activity (MA) (mA mg^{-1}) at a given overpotential was obtained by:

$$MA = j/m_s \quad (5)$$

Where j is the current density (A cm^2), and ms is the total catalyst mass on theelectrode (g cm^2)

The intrinsic catalytic activity of catalysts was assessed by calculating turnoverfrequency (TOF), defined as:

$$TOF = (A*J) / (4*F*m) \quad (6)$$

where A is the geometric surface area (cm^2) of the electrode, j is the current density (Acm^{-2}), F. is the- Faraday constant (96485 C. mol^{-1}), and m is molar quantity ofelectrochemically active sites (mol). The factor of 4 corresponds to the four-electrontransfer required for the evolution of one O_2 molecule during the oxygen evolution reaction.

The number of active sites (m) was estimated from CV data by analyzing the lineardependence of anodic peak current (i_a) on scan rate (v), assuming a surface-controlledone-electron redox process (n=–1). The relationship is described-as:

$$Slope = (n^2*F^2*m)/(4*R*T)$$

where R is the gas constant (8.314-J mol^{-1} K^{-1}) and T is the absolute temperature (K).

The Faradaic efficiency (FE) for H_2 and O_2evolution was calculated by:

$$FE = V_{theo}/V_{exp}$$

where V_{theo} and the V_{exp} are the experimentally measured and theoretically calculated gas volumes (mL), respectively. The theoretical gas volume was obtained from:

$$V_{theo} = V_m*Q/(n*F)$$

where V_m is the molar volume of an ideal gas at standard conditions (22.4 L mol^{-1}), Q is the total charge passed (C), n is the number of electrons involved in the reaction (n = 4 for OER; n = 2 for HER), and F is the Faraday constant (96485-C mol^{-1}).

Computational details

All the calculations were performed in the framework of the density functional theory with the projector augmented plane-wave method, as implemented in the VASP.[1] The generalized gradient approximation proposed by Perdew, Burke, and Ernzerhof was selected for the exchange-correlation potential.[2] The van der Waals interaction was described by the DFT-D3 approach.[3] The cut-off energy for plane wave was set to 400 eV. The energy criterion was set to 10^{-5} eV in iterative solution of the Kohn-Sham equation. A vacuum layer of 15 Å was added perpendicular to the sheet to avoid artificial interaction between periodic images. The Brillouin zone integration was performed using a 2 * 2 x 1 K-mesh. All the structures were relaxed until the residual forces on the atoms have declined to less than 0.02 eV/Å. Based on the XRD data, we used the structures of xxx with lattice constant Ni_3S_2 and $CoMo_2S_4$ with lattice constant $Ni_3S_2/CoMo_2S_4$ as the catalyst crystal structures, respectively.

The lattice constant information is as follows:

Ni_9S_6		$Co_2Mo_4S_8$	
Space Group: P 1 (#1-1)		Space Group: P 1 (#1-1)	
a= 5.67382	α=90.0000°	a= 12.39623	α=90.0000°
b= 5.67382	β=90.0000°	b= 3.20733	β=114.8357°
c= 7.04707	γ=120.0000°	c= 5.93825	γ=90.0000°

In addition, to evaluate the HER and OER activity, the Gibbs free energy of intermediate adsorbed on catalyst was considered and the calculation method follows our previously published works.[4]

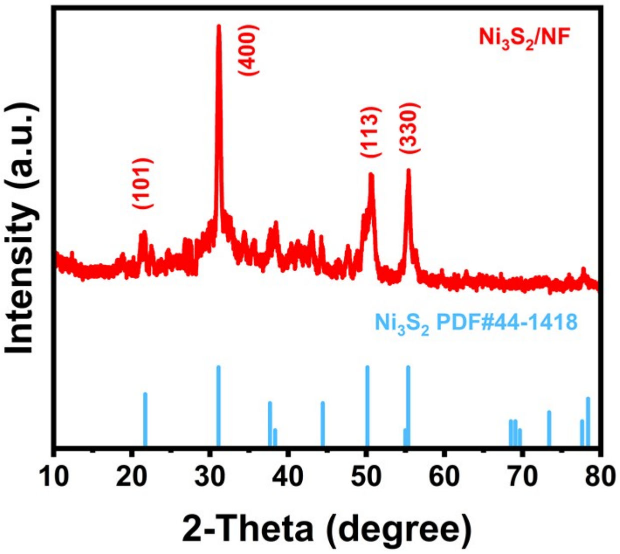

Figure S1. XRD pattern of Ni_3S_2/NF.

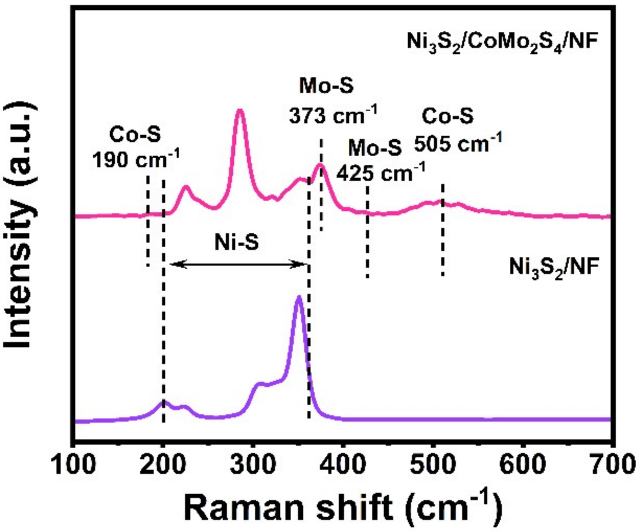

Figure S2. Raman spectra of $Ni_3S_2/CoMo_2S_4/NF$, Ni_3S_2/NF.

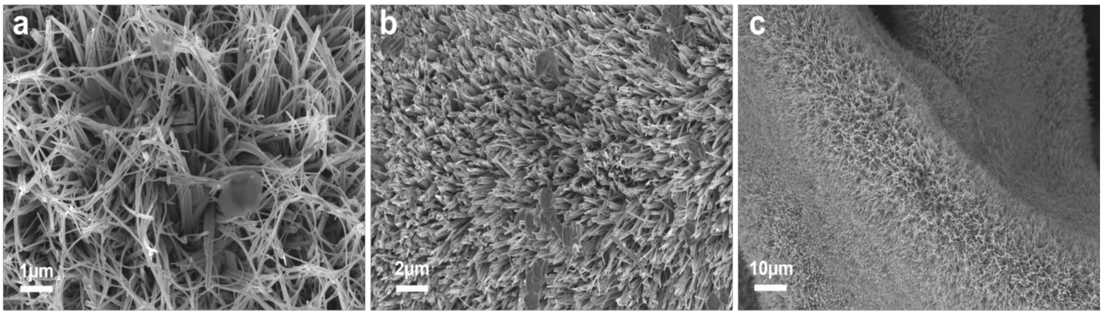

Figure S3. SEM images of $Ni_3S_2/CoMo_2S_4/NF$.

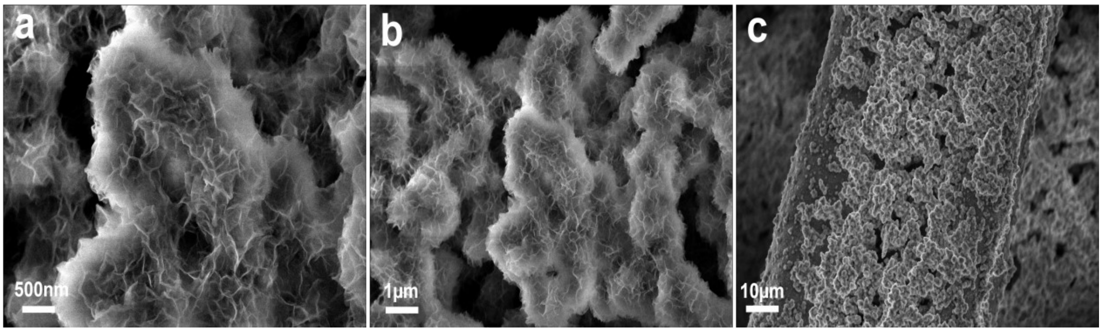

Figure S4. SEM images of Ni_3S_2/ NF.

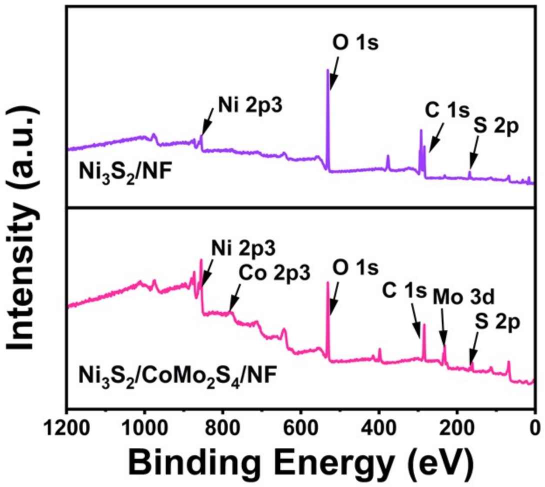

Figure S5. XPS core level spectra of $Ni_3S_2/CoMo_2S_4$/NF, and Ni_3S_2/NF.

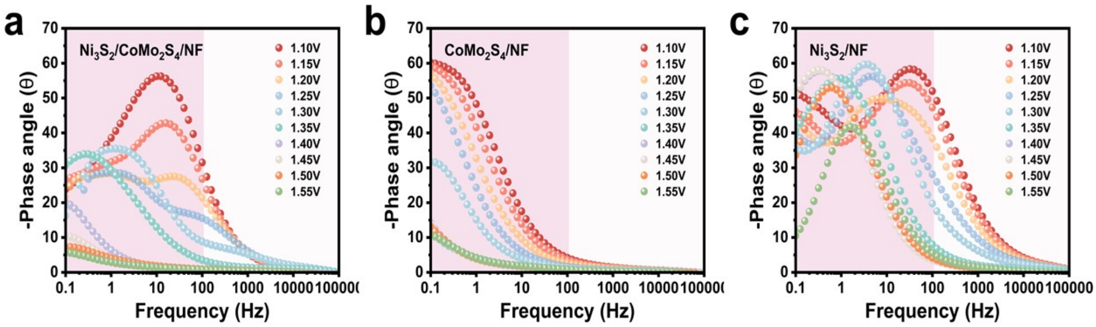

Figure S6. Bode plots of $Ni_3S_2/CoMo_2S_4$/NF, $CoMo_2S_4$/NF and Ni_3S_2/NF recorded at different potentials during the OER.

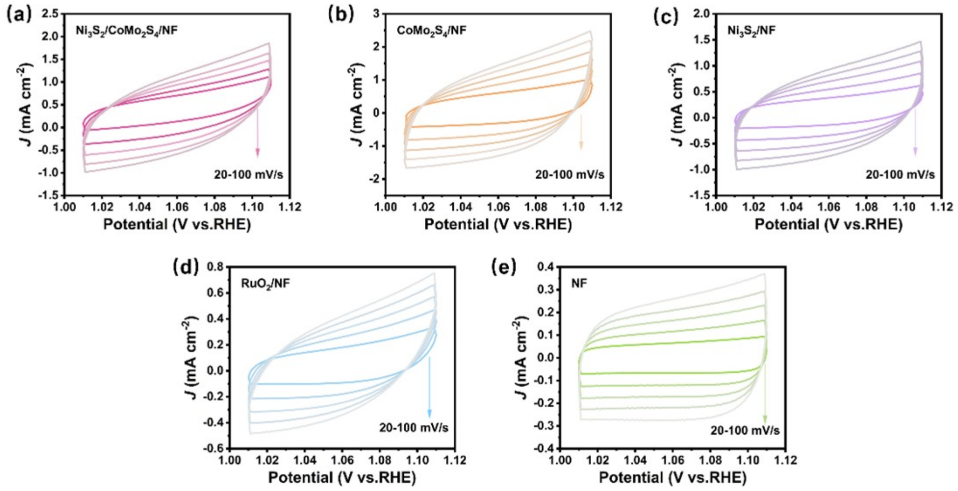

Figure S7. Cyclic voltammetry (CV) curves of (a) $Ni_3S_2/CoMo_2S_4/NF$, (b) $CoMo_2S_4/NF$, (c) Ni_3S_2/NF, (d)RuO_2/NF. and (e) NF recorded at scan rates ranging from 20 to 100 mV s^{-1}.

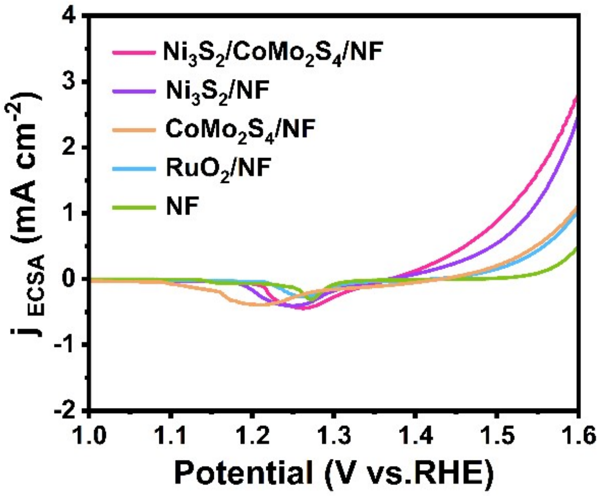

Figure S8. LSV curves normalized by ECSA.

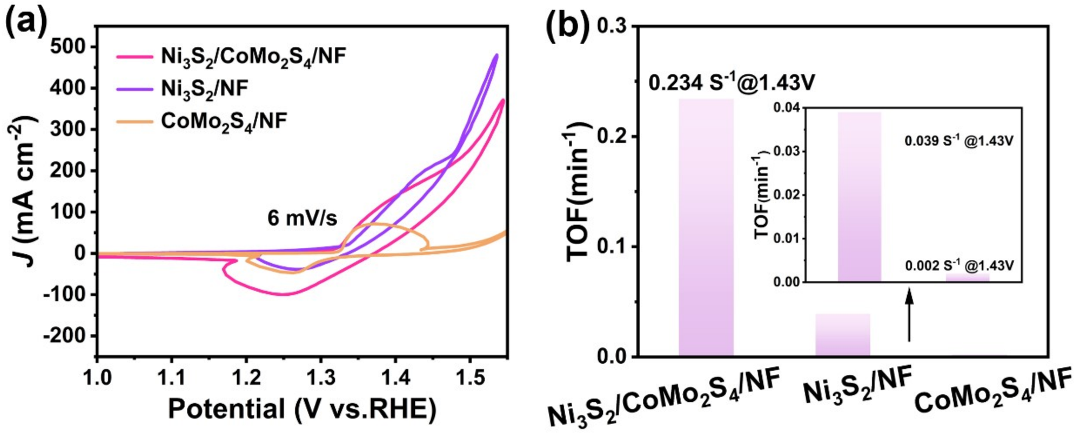

Figure S9. (a) Cyclic voltammetry (CV) curves of Ni_3S_2/$CoMo_2S_4$/NF、$CoMo_2S_4$/NF and Ni_3S_2/NF, (b) TOF of Ni_3S_2/$CoMo_2S_4$/NF、$CoMo_2S_4$/NF and Ni_3S_2/NF at 6 mV/s.

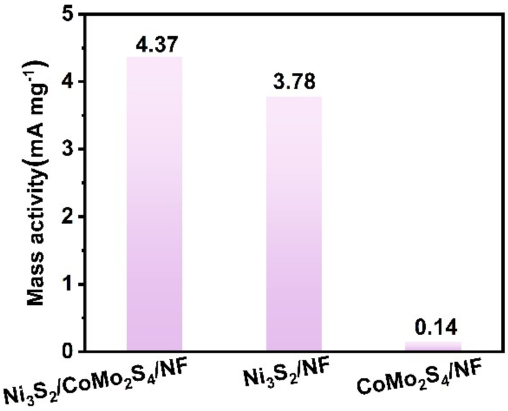

Figure S10. Mass activity of Ni_3S_2/$CoMo_2S_4$/NF、$CoMo_2S_4$/NF and Ni_3S_2/NF.

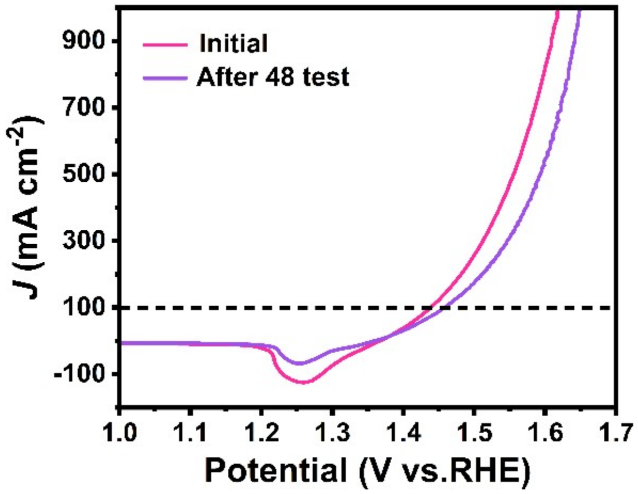

Figure S11. Polarization curves recorded after 48 test.

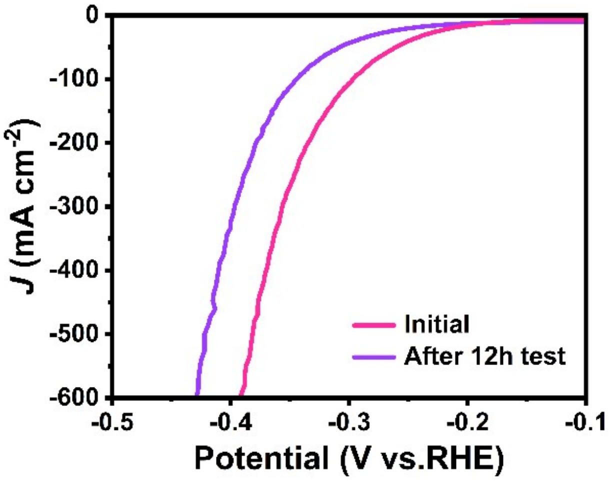

Figure S12. Polarization curves recorded after 12 test.

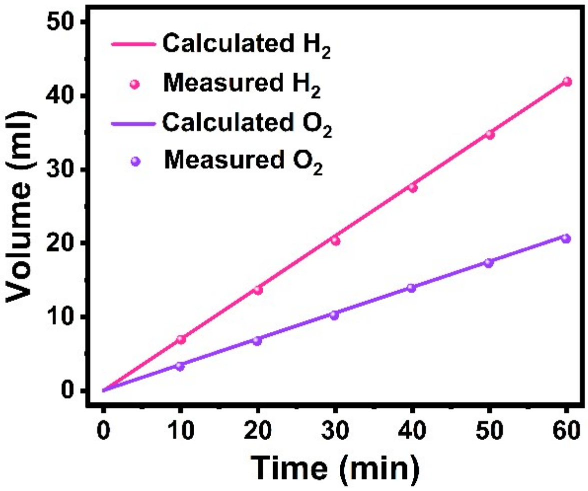

Figure S13. Experimental and theoretical H_2/O_2 gas volumes generated within 1 h at 100 mA cm^{-2}.

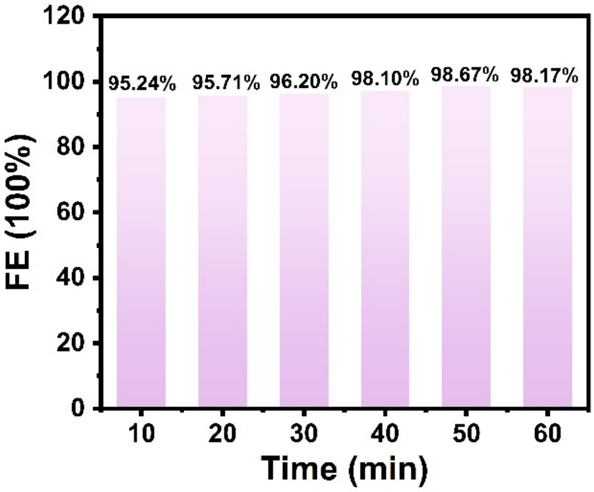

Figure S14. Faraday efficiency values of the $Ni_3S_2/CoMo_2S_4$/NF at different time periods.

Figure S15. Photograph of the two-electrode electrochemical cell and the corresponding electrodes.

b

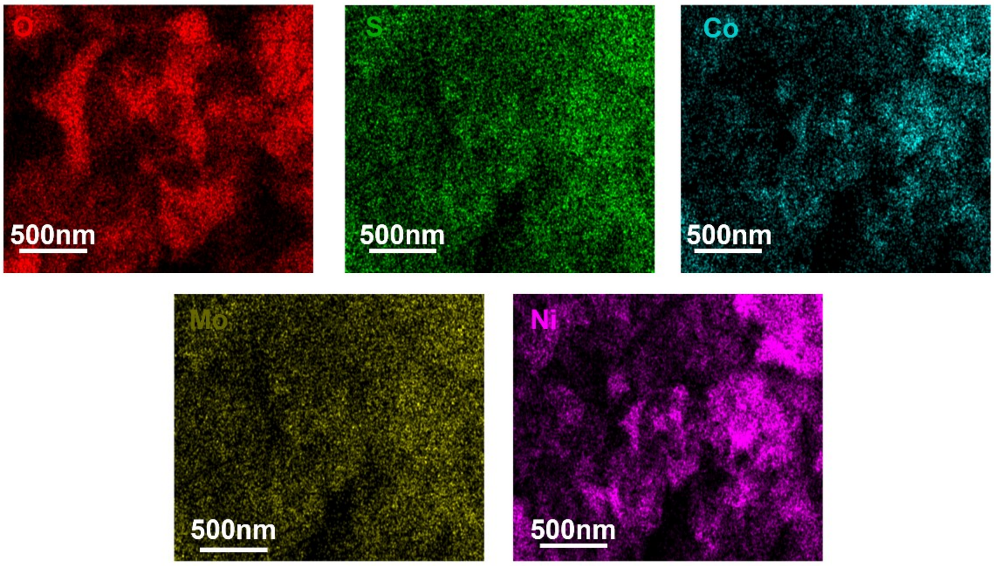

Figure S16. SEM image and the corresponding elemental mapping of $Ni_3S_2/CoMo_2S_4$/NF after the OER stability test.

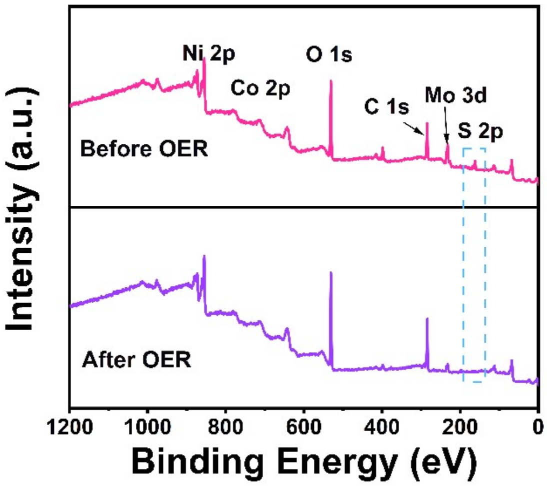

Figure S17. XPS spectra of $Ni_3S_2/CoMo_2S_4/NF$ before and after the OER stability test.

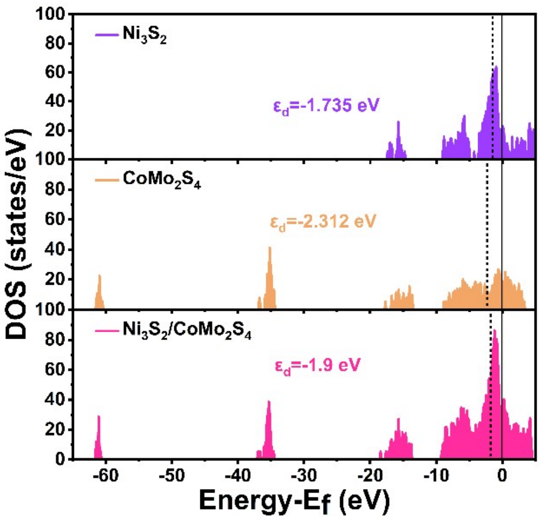

Figure S18. DOS plots of Ni_3S_2, $CoMo_2S_4$ and $Ni_3S_2/CoMo_2S_4$ during the OER.

Table S1. Elemental composition (Ni, Mo, Co and S) of $Ni_3S_2/CoMo_2S_4/NF$ catalysts determined by ICP-OES.

Catalysts	**ICP-OES**				
	Ni (at.%)	**Mo (at.%)**	**Co (at.%)**	**S (at.%)**	**C\O(at.%)**
$Ni_3S_2/CoMo_2S_4/NF$	77.3	5.81	1.2	6.22	9.01

Table S2. Comparison of the OER performance of $Ni_3S_2/CoMo_2S_4$/NF with previously reported electrocatalysts.

Electrocatalyst	**Substrate**	**η_{100} (mV)**	**Tafel (mV dec^{-1})**	**Ref.**
$Ni_3S_2/CoMo_2S_4$/NF	Ni foam	202	49	This work
Ce-FeS_2/Ni_3S_2	Ni foam	330	100	5
Ni_3S_2-$Fe_5Ni_4S_8$	NiFe foam	240	48.1	6
NiFe/NF	Ni foam	402	120	7
Ni_3Se_2/Ni_3S_2/NF	Ni foam	312	145.54	8
Ni_3S_2	Ni foam	356	210.42	9
Ni_3S_2-W-Vs	Ni foam	246	66	10
a-CoS/Ni_3S_2	Ni foam	248	53	11
N-CoS_2	Ni foam	292	55	12
$CoNi_2S_4$（$CoNi_2S_4$/Ni）	Ni foam	328	160	13
FeCo-Ni_3S_4	Ni foam	279	63.2	14
NixSy@MnOxHy	Ni foam	326	39	15
PtFeCoNiCu	Ni foam	264	84	16
MoS_2@rGO	Ni foam	303	92	17
FeCoCuCrNi-MoS_2-MoP	Ni foam	234	103.9	18
$CuNiCoS_4$ /1T-MoS_2	Ni foam	230	126	19

Table S3. Comparison of the HER performance of $Ni_3S_2/CoMo_2S_4/NF$ with previously reported electrocatalysts.

Electrocatalyst	**Substrate**	**η_{10} (mV)**	**Tafel (mV dec^{-1})**	**Ref.**
$Ni_3S_2/CoMo_2S_4/NF$	Ni foam	202	100	This work
$CoMoS_4/CC$	Carbon cloth	143	105	[19]
Co_3Mo_2-LDH	Ni foam	165	88	[20]
$C@Mo_2C/Co$	Carbon cloth	145	90.7	[21]
$CoMoS_4$	Ni foam	141	60.1	[22]
$MoS_2/NiS_2/CoS_2$	Ni foam	101	116	[23]
$MoS_2/(CoNi@G)$	Ni foam	150	66	[24]
Mo-CoS_2/NC	Carbon cloth	158	65	[25]
H-Fe-CoMoS	Carbon paper	137	98	[26]
Cu-Ni_3S_2	Ni foam	121	86.2	[27]
$Co_{0.5}MoS_2/N$	Ni foam	178	63.8	[28]
Fe-$MoS_2/CoMo_2S_4$	Carbon paper	122	90	[29]
$CoMo_2S_4$	Ni foam	162	116	[30]

Table S4. Comparison of overall cell performance of $Ni_3S_2/CoMo_2S_4/NF$ and previously reported electrocatalysts at a current density of 10 mA cm^{-2}.

Electrocatalyst	**Cell voltage (V)**	**Ref.**
$Ni_3S_2/CoMo_2S_4/NF$	1.50	This work
$Pt\text{-}CoS_2/CC$	1.55	[31]
CS-NFO@PNC-700	1.66	[32]
FeCoP/NF	1.68	[33]
$NiCo_2S_4NA/CC$	1.68	[34]
$MoS_2\text{-}Ni_3S_2HNRs/NF$	1.52	[35]
$CoSAs\text{-}MoS_2/TiNNRs$	1.65	[35]
$NiFe\text{-}LDH/NiCo_2O_4/NF$	1.60	[36]
$Ni/Mo_2C\text{-}PC/NF$	1.66	[37]
$Co_{0.50}Fe_{0.50}S/rGO@NF$	1.66	[38]
FeCoNiCuPd/CC	1.52	[39]
Co-P/NC/CC	1.85	[40]

References:

1 G. Kresse and D. Joubert, *Phys. Rev. B.,* 1999, **59**, 1758-1775.

2 J. Perdew, K. Burk and M. Ernzerhof, *Phys. Rev. Lett.,* 1996, **77**, 3865-3868.

3 S. Grimme, J. Antony, S. Ehrlich and H Krieg, *J. Chem. Phys.,* 2010, **132**,154104.

4 R. Ren, J. Wang, Y. Xie, T. Li, H. Wei, F. Wang, H. Yang, Z. Lin and J. Gao, *Appl. Catal. B-Environ.,* 2026, **388**, 126543.

5 Y. He, K. Shi, X. Wang, X. Zheng, L. Luo, L. Lin, Z. Sun and G. Sun, *Inorg. Chem. Front.,* 2024, **21** ,7623-7632.

6 Y. Wu, Y. Li, Z. Lü, L. Xu and B. Wei, *J. Mater. Sci.,* 2020, **55**, 15963-15974.

7 Y. Wu, R. Su, Y. Li, Z. Wang, Z. Lü, L. Xu and B. Wei, *Electrochim. Acta.,* 2019, **309**, 415-423.

8 M. Lin, M. Gu, X. Deng, Q. Xi and X. Zhan, *Chem. Eng. J.,* 2023, **468**, 143705.

9 Z. Wang, S. Shen, Z. Lin, W. Tao, Q. Zhang, F. Meng, L. Gu and W. Zhong, *Adv. Funct. Mater.*, 2022, **32**, 2112832.

10 W. Luo, Y. Yu, Y. Wu, W. Wang, Y. Jiang, W. Shen, R. He, W. Su and M. Li, *Small.,* 2024, **20**, 2310387.

11 W. Zhang, W. Chen, Q. Xiao, L. Yu, C. Huang, G. Lu, A. Morawski and Y. Yu, *Appl. Catal. B-Environ.,* 2020, **268**, 118449.

12 J. Li, Q. Zhuang, P. Xu, D. Zhang, L.Wei *and* D. Yuan, *Chin. J. Catal.,* 2018, **39**, 1403-1410.

13 X. Mao, Y.Liu, Z. Chen, Y. Fan *and* P. Shen, *Chem. Eng. J.,* 2022**, 427**, 130742.

14 P. Wang, Y. Luo, G. Zhang, Z. Chen, H. Ranganathan, S. Sun and Z. Shi, *Nano-Micro Lett.,* 2022, **14**, 120.

15 S. Maria, N. Jeghan, J. Kim and G. Lee, *APPL SURF SCI.,* 2021, **546**, 149072.

16 F. Wang, S. Chen, Z. Tong, X. Liu, H. Zhou, Y. He, G. Shu, Y. Jin and W. Zheng, *ACS Appl. Mater. Interfaces.,* 2025, **49**, 66617–66629.

17 U. Afreen, U. Afreen and N. K. Singh, *J. Mater. Chem. A.,* 2025, **15**, 10945–10966.

18 G. Amarjeet, M. Karthick, T. S. Kumar, S. Prabu, M. Vinu and T, *Int. J. Hydrogen Energy.,* 2026, **203**, 153124.

19 J. Shen, Y. Liu, Q. Chen, W. Yu and Q. Zhong, *J. Colloid Interface Sci.,* 2024, **658**, 1009–1015.

20 L. Xia, X. Zhang, H. Song, Y. Zheng, X. Li, B. Gao, K. Huo and P. Chu, *J. Hydrogen Energy.*, 2020, **45**, 22629-22637.

21 A. Yadav, Y. Hunge and S. Kang, *Ultrason. Sonochem.,* 2021, **72**, 105454.

22 Z. Yin, X. Liu, S. Chen, H. Xie, L. Gao, A. Liu, T. M and Y. Li, *Mater.Today Nano.,* 2022, **17**, 100156.

23 Y. Tu, J. Deng, C. Ma, L. Yu, X. Bao and D. Deng, *Nano Energ.,* 2020, **72**, 104700.

24 L. Zhao, C. Gong, X. Chen, X. He, H. Chen, X. Du, D. Wang, W. Fang, H. Zhang and W. Li, *APPL SURF SCI.,* 2023, **623**, 157030.

25 Y. Guo, X. Zhou, J. Tang, S. Tanaka, Y. Kaneti, J. Na, B. Jiang, Y. Yamauchi, Y. Bando and Y. Sugahara, *Nano Energ.,* 2020, **75**, 10491.

26 L. Zhang, X. Gao, Y. Zhu, A. Liu, H. Dong, D. Wu, Z. Han, W. Wang, Y. Fang, J. Zhang, Z. Kou, B. Qian and T. Wang, *Nanoscale.*, 2021, **13**, 2456-2464.

27 S. Selem, H. Hasaniena and A. El‐Fergany, *Int. J. Energy Res.*, 2020, **44**, 4629-4640.

28 Y. Guo, J. Tang, J. Henzie, B. Jiang, W. Xia, T. Chen, Y. Bando, Y. Kang, M. Hossain, Y. Sugahara and Y. Yamauchi, *ACS Nano.*, 2020, **14**, 4141-4152.

29 H. Wang, X. Li, N. Qin, X. Zhao, H. Cheng, G. Cao and W. Zhang, *J. Mater. Chem. A.*, 2019, **7**, 12068-12074.

30 X. Han, X. Wu, Y. Deng, J. Liu, J. Lu, C. Zhong and W. Hu, *Adv. Energy Mater.*, 2018, **8**, 1800935.

31 S. Ramakrishnan, D. Velusamy, S. Sengodan, G. Nagaraju, D. Kim, A. Kim and D. Yoo, *Appl. Catal. B-Environ.*, 2022, **300**, 120752.

32 K. Sun, K.Wang, T. Yu, X. Liu, G. Wang, L. Jiang, Y. Bu and G. Xie, *Int. J. Hydrog. Energy.*, 2019, **44**, 1328-1335.

33 D. Liu, Q. Lu, Y. Luo, X. Sun and A. Asiri, *Nanoscale.*, 2015, **7**, 15122-15126.

34 Y. Yang, K. Zhang, H. Lin, X. Li, H. Chan, L. Yang and Q. Gao, *ACS Catal.*, 2017, **7**, 2357-2366.

35 T. Doan, D. Nguyen, S. Prabhakaran, D. Kim, D. Tran, N. Kim and J. Lee, *Adv. Funct. Mater.*, 2021, **31**, 2100233.

36 Z. Wang, S. Zeng, W. Liu, X. Wang, Q. Li, Z. Zhao and F. Geng, *ACS Appl. Mater. Interfaces.*, 2017, **9**, 1488-1495.

37 Z. Yu, Y. Duan, M. Gao, C. Lang, Y. Zheng and S. Yu, *Chem. Sci.*, 2017, **8**, 968-973.

38 K. Zhang, P. Jiang, Q. Gu, Y. Leng, P. Zhang, Z. Li and Y. Li, *Int. J. Energy Res.*, 2022, **46**, 7320-7333.

39 Y. Liao, R. Zhu, W. Zhang, H. Zhu, Y. Sun, J. Chen, Z. Dong and R. Lv, *Nano Res.*, 2024, **17**, 3379-3389.

40 X. Liu, J. Dong, B. You and Y. Sun, ***RSC Adv.***, 2016, **6**, 73336-73342.